



Supplement of

Biogeochemical dynamics of the sea-surface microlayer in a multidisciplinary mesocosm study

Riaz Bibi et al.

Correspondence to: Riaz Bibi (riaz.bibi@uol.de)

The copyright of individual parts of the supplement might differ from the article licence.

1 **Sect. S1: Pilot study mixing experiment**

2 A mixing experiment was conducted with four set-up configurations of small flow pumps (ATK-4 Wavemaker
3 24V – 18 m³ h⁻¹) in the SURF to determine the optimal configuration for a well-mixed basin with minimal capillary
4 wave movement at the surface. Flow pumps were mounted on metal stands attached with metal clamps and hex
5 jam nuts (Fig. S1) that could be loosened, opened, or closed to adjust the distance to the bottom of the SURF basin.
6 Out of a total of eight flow pumps, one was placed in each corner of the basin facing towards the next corner,
7 counterclockwise, and two were placed on each long side of the basin, close to the wall facing counterclockwise.
8 Flow pumps had a digital touch controller to control and adjust the flow speed to make waves from 0 –100 in
9 increments of 10. The flow angle of the pumps was also adjustable, and it was set to stay at an angle of 0° - 25°
10 up, where 0° is the axis perpendicular to the metal stand and parallel to the ground.

11 A comprehensive set of measurements was carried out with a FerryBox (PocketBox, 4H-Jena) for key parameters,
12 including phytoplankton biomass (Chlorophyll-a, Chl_a) and turbidity, to determine the homogeneity of the water
13 column in SURF. The FerryBox inflow tube was inserted at different measuring points (Fig. S2) within the basin
14 at the surface (about 20 cm depth) and at the bottom (about 30 cm off the ground). The exact measuring points
15 within the basin were very similar for each configuration set-up and were always spread throughout the basin. The
16 FerryBox measures every 5 s. Therefore, the duration of the inflow tube in the pool was set between 1–2 min to
17 get an average value. The measurements of the configurations were then conducted after waiting at least an hour
18 for the mixing process to occur. Table S1 displays the set-up configurations for the pumps and the obtained mean
19 value, number of measurements, and standard deviation of the measured Chl_a and turbidity values at all measured
20 points. Initial ground state values of Chl_a and turbidity were measured without any mixing actions with pumps
21 before starting.

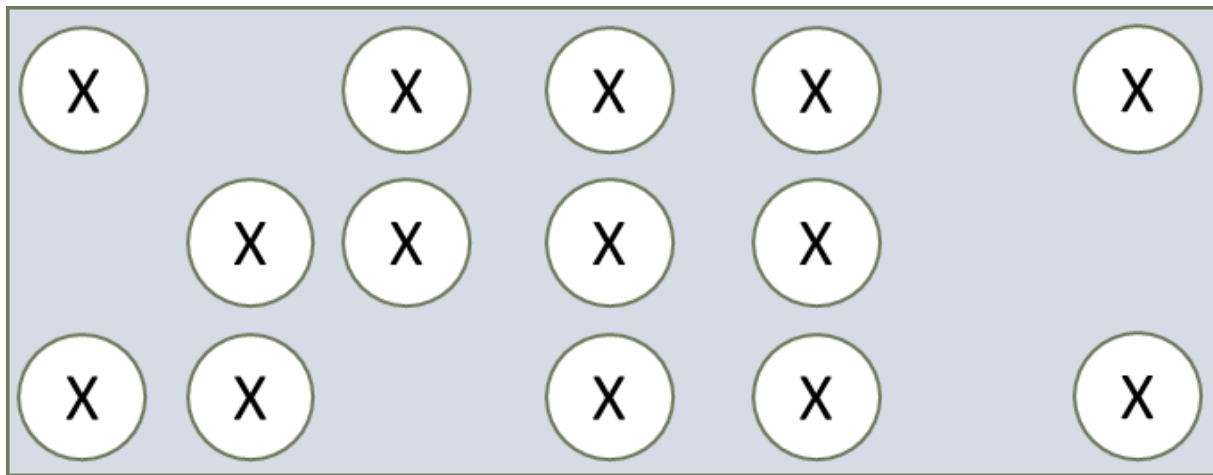
22



23

24 **Figure S1** An image of one of the flow pumps mounted on the metal stand.

25



26

27 **Figure S2** Schematic representation of measuring points of the FerryBox in SURF from a top-down perspective.

28 **Table S1** Chl_a and turbidity measured at different sampling points for different pumps configurations within the
 29 basin during the pilot phase. Their mean value (μ), number of measurements (N), and standard deviation (SD) are
 30 displayed together with the height, flow speed, and configuration of the pumps.

Configuration no.	Height of pump on metal stand (23.5 cm)	Flow Speed of pump	Pump configuration in SURF pool	Chl _a	Turbidity
				μ	μ
				N	N
				SD	SD
0	-	0		1.17	278.79
				6	4
				0.06	214.89
1	High	100		2.70	116.42
				7	7
				0.05	2.25
2	Low	10		3.44	106.28
				9	9
				0.11	0.38
3	Low	10		2.87	207.29
				20	19
				1.43	112.33
4	Low	20		1.88	122.34
				12	12
				0.09	68.09

31

32 **Sect. S2: Surfactant Coverage Index**

33 Spectral signatures of C-H stretch vibrations in vibrational sum-frequency generation (VSFG) spectra can be used
 34 for the quantification of surface-active molecules with alkyl chain functionalities. Referencing the measured
 35 spectral intensity to the VSFG spectrum of a well-defined monolayer of a reference with complete surface coverage
 36 allows one to define a *surface coverage* index sc . The operationally defined sum parameter sc is helpful to
 37 characterize the state of natural air-water interfaces with respect to the effective coverage with surface-active
 38 organic substances, which plays a key role in describing the influence of surfactants on wave-damping and thus
 39 air-sea gas exchange. In contrast to the already widely used *surfactant concentration* (or *surfactant activity*)
 40 parameter, which is a measure for surfactant abundance in the entire SML on a micrometer scale (AC voltammetry,
 41 expressed in terms of μg Triton X-100 equivalent L^{-1} , μg Teq L^{-1}), the surface coverage index characterizes the
 42 presence of a molecular film of surfactants directly at the air-water interface on a nanometer scale. The use of
 43 VSFG for investigating the surface of natural water bodies has been pioneered by Koronowski et al. (1993) and
 44 has been further developed for SML characterization by Friedrichs and coworkers (Laß et al., 2011; Laß et al.,
 45 2011; Lange, 2021), including applications in SML time-series measurements (Laß et al., 2013) and the study of
 46 the microbial control of the SML surfactant state (Engel et al., 2018).

47 VSFG spectroscopy is a non-linear laser spectroscopic method to investigate molecular films at interfaces (Buck
 48 and Himmelhaus, 2001). It is inherently surface-sensitive due to the underlying spectroscopic selection rules of
 49 sum frequency generation (SFG) and only probes molecules present directly at the air-water interface on a
 50 molecular scale. In simple terms, SFG is the combination of two photons, one resonant with a molecular vibration,
 51 yielding a third photon that is detected as the signal. This non-linear process can only occur in a non-inversion
 52 symmetric environment, hence explaining the surface sensitivity of the method. Only molecules with preferential
 53 molecular alignment at the interface yield signal, where SFG signal intensity is proportional to the square of the
 54 second-order susceptibility $\chi^{(2)}$, $I_{\text{SFG}} \propto (\chi^{(2)})^2$. It can be interpreted as the macroscopic average of the molecular
 55 hyperpolarizabilities β such that the overall SFG intensity is proportional to the number of probed SFG active
 56 molecules N squared: $I_{\text{SFG}} \propto (\beta \times N)^2$. Next to the N^2 dependence, due to changes of the overall molecular
 57 orientation of the probed molecules, β may depend on the surfactant surface concentration as well. However, it
 58 has been shown for natural SML samples that beta, and with it the measured spectral C-H signatures, are largely
 59 independent of the surfactant abundance (Laß et al., 2011).

60 Therefore, the resulting square root relationship between N and the measured intensity leads directly to the
 61 operational definition of the surface coverage index:

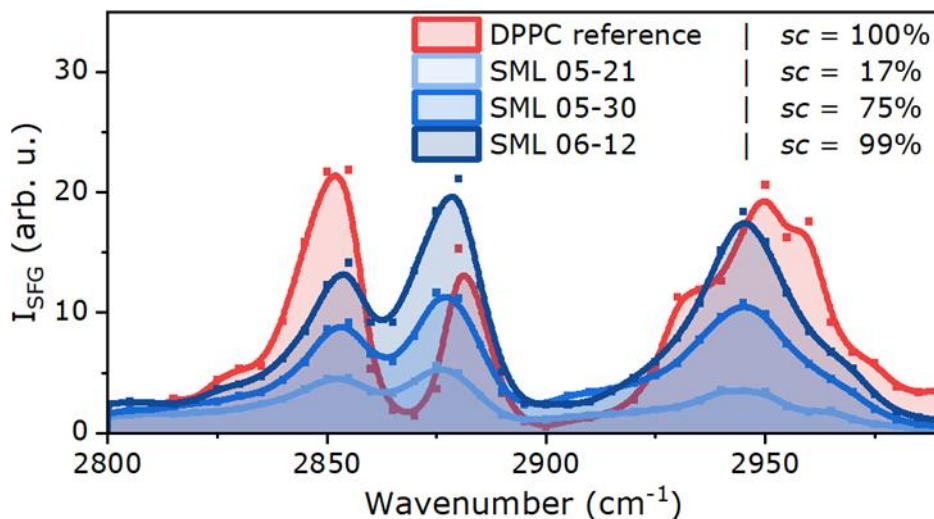
62

$$63 \quad sc = \frac{\sqrt{\int_{2800 \text{ cm}^{-1}}^{3000 \text{ cm}^{-1}} I_{\text{SML}}(\tilde{\nu})d\tilde{\nu}} - \sqrt{\int_{2800 \text{ cm}^{-1}}^{3000 \text{ cm}^{-1}} I_{\text{H}_2\text{O}}(\tilde{\nu})d\tilde{\nu}}}{\sqrt{\int_{2800 \text{ cm}^{-1}}^{3000 \text{ cm}^{-1}} I_{\text{DPPC Reference}}(\tilde{\nu})d\tilde{\nu}} - \sqrt{\int_{2800 \text{ cm}^{-1}}^{3000 \text{ cm}^{-1}} I_{\text{H}_2\text{O}}(\tilde{\nu})d\tilde{\nu}}}$$

64 Here, the nominator reflects the signal of the natural SML sample and the denominator the monolayer signal of
 65 the reference substance dipalmitoylphosphatidylcholine (DPPC) with a surface concentration of $0.22 \text{ nmol cm}^{-2}$
 66 (corresponding to a surface pressure of 3.0 mN m^{-1}), representing the state of a 100 % covered surface. Both are
 67 corrected for the residual signal of a surfactant-free water background spectrum. In this way, surface coverage

68 index values of $sc = 0\%$ or $sc = 100\%$ can be interpreted as a surfactant-free or a fully covered molecular film of
69 surfactant-like material directly at the air–sea interface, respectively.

70 Example spectra are shown in Fig. S3 for three SML samples with increasing surface coverage values in
71 comparison with the spectrum of the DPPC reference. Measurements of the SML samples were conducted in a
72 circular Teflon dish with a surface area of 20 cm^2 and a spectral resolution of 5 cm^{-1} , and the DPPC sample was
73 analyzed with a Langmuir trough, with the surface pressure measured using a Wilhelmy balance. Details of the
74 commercial picosecond VSFG spectrometer (EKSPLA, 532 nm up-conversion wavelength) can be found in Laß
75 and Friedrichs (2011) and Engel et al. (2018). Note that the spectra of the SML samples in Fig. S3 show different
76 overall signal intensity, but the relative signal intensities of the observed vibrational bands remain largely
77 unchanged, supporting that possible intensity variations related to β are minor (see above). In contrast to well-
78 defined monolayers of single insoluble (dry) surfactants or soluble (wet) surfactants (the latter in adsorption
79 equilibrium with the underlying bulk phase), natural surface films can be considered mixed films with
80 contributions from different biosurfactants, biopolymers, and colloids forming complex interfacial structures.



81
82 **Figure S3 Exemplary data for the determination of the surface coverage index, sc . Three VSFG spectra of mesocosm**
83 **samples with increasing sc value in comparison with the reference spectra of a DPPC (dipalmitoylphosphatidylcholine)**
84 **monolayer with a surface concentration of 0.22 nmol cm^{-2} .**

85 Sect. S3: Interlab Comparison of Dissolved Organic Carbon (DOC) and Total Dissolved Nitrogrn (TDN)

86 Two laboratories assessed DOC concentrations, which were merged to receive a better data coverage and higher
87 accuracy. Differences in handling the samples are described and briefly discussed in the subsequent paragraphs.

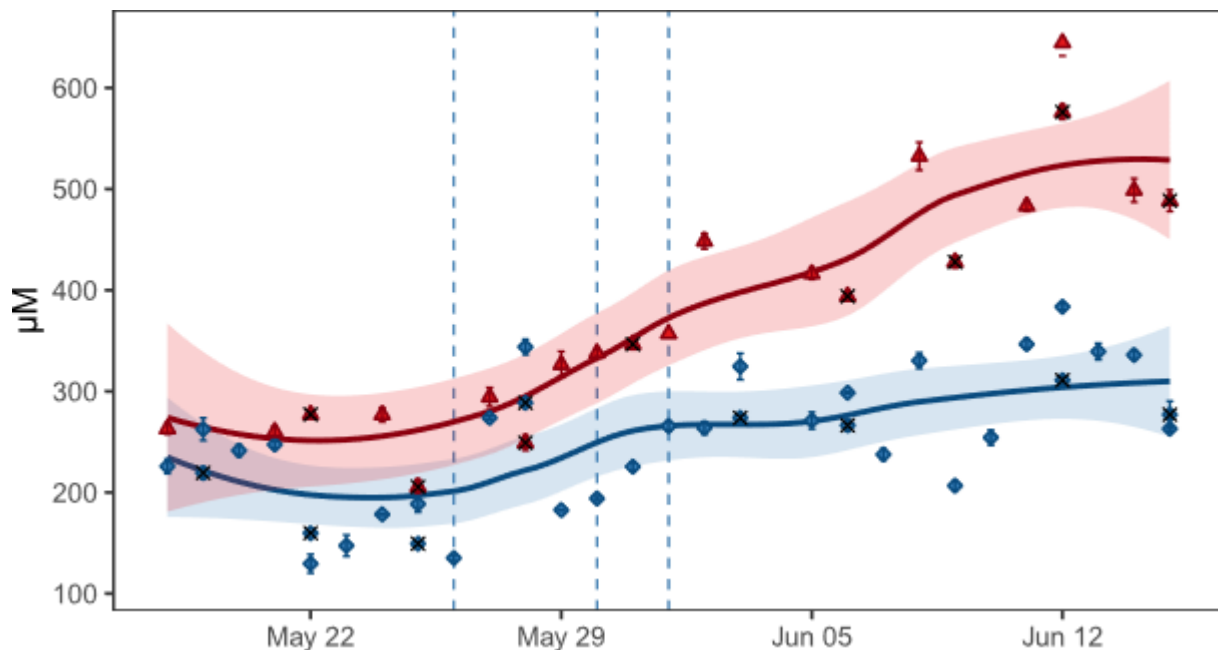
88 Samples of ICBM, Oldenburg were primarily filtered through combusted GFF filters (4 hours at $450\text{ }^\circ\text{C}$, Whatman,
89 $0.7\text{ }\mu\text{m}$). To increase sample numbers, additional water samples were provided from a parallel set, filtered under
90 vacuum through a reusable polysulfone bottle-top filter holder (Thermo Scientific Nalgene, US) containing
91 polycarbonate filters ($5.0\text{ }\mu\text{m}$, $3.0\text{ }\mu\text{m}$ and finally $0.2\text{ }\mu\text{m}$, 47 mm diameter, Nuclepore Track-Etch Membrane,
92 Whatman, UK). These polycarbonate filters were subsequently used by other members of the BASS research unit
93 to collect microbial cells for community analyses. The samples were stored at natural pH in acid-rinsed HDPE
94 bottles at $-18\text{ }^\circ\text{C}$. After thawing and sonication, 2 mL aliquots were transferred into combusted 20 mL glass vials,
95 diluted to 10 mL with low-carbon ultrapure water acidified to pH 2 with HCl (ACS or p.a. quality, 32%). DOC
96 concentrations were measured using a Shimadzu TOC Analyser (TOC-L or TOC-VCPH) following the high-
97 temperature catalytic oxidation method (Sugimura and Suzuki, 1988). Each sample was injected four times, and
98 outliers were removed. A run was considered valid if the DOC in the reference material remained between 41-44

99 $\mu\text{mol L}^{-1}$, with a precision better than 5%. For calibration of DOC, 12 different concentrations of an L-arginine
100 standard (Sigma, USA) were prepared and checked against a potassium hydrogen phthalate standard (Nacalai
101 Tesque, Japan).

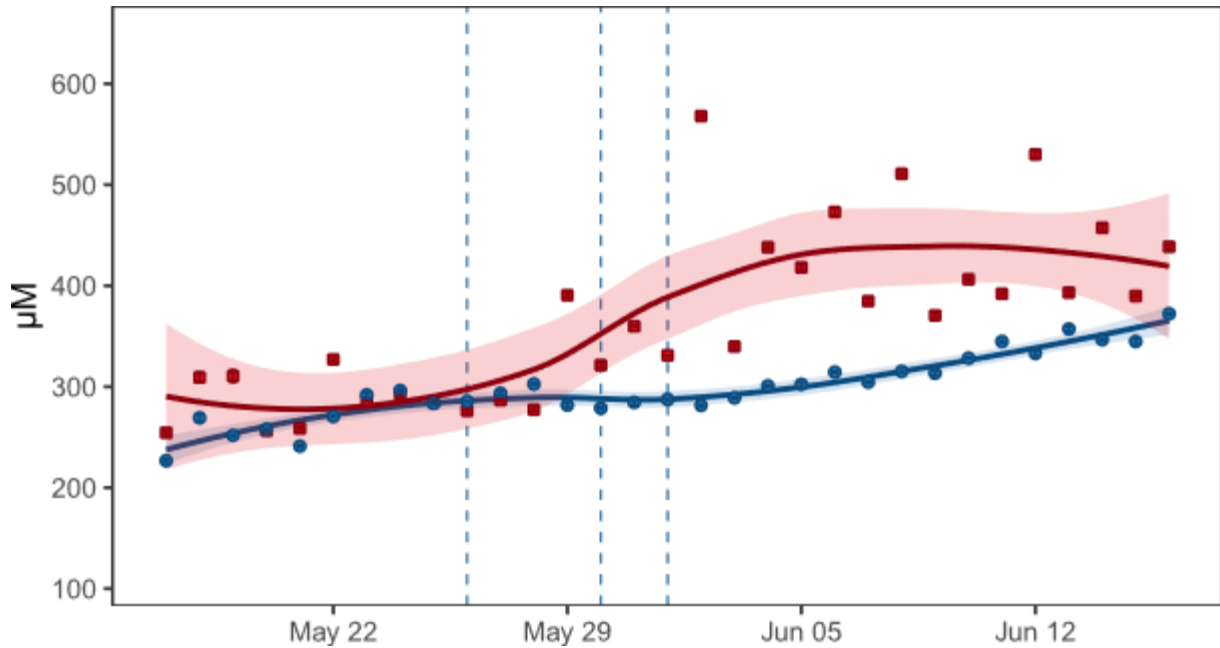
102 The second sample set was prepared for DOC and additional TDN quantification at GEOMAR, Kiel. Samples in
103 duplicates were filtered through sterile and pre-rinsed $0.45 \mu\text{m}$ glass microfiber filters syringe filters (GMF GD/X
104 Whatman, GE Healthcare Life Sciences) into 20 mL ampules, which were pre-combusted (8 hours at 500°C). 20
105 μL of 30% HCl (Suprapure, Sigma-Aldrich) was added to acidify the samples, which were then immediately sealed
106 and stored at $+4^\circ\text{C}$ until analysis. One duplicate was measured repeatedly ($n=4$), also using a high-temperature
107 catalytic oxidation analyser (TOC-VCSH, Shimadzu). Sample specific precision was calculated as the standard
108 deviation between the four repeated measurements divided by the mean and showed a relative standard deviation
109 (relSD) of $0.54 \pm 0.30\%$ for DOC and $1.45 \pm 0.60\%$ for TDN. (The maximum relSD of repeated measurements for
110 DOC was 1.99% and for TDN 2.87%.) For calibration of DOC and TDN, respectively, five and four different
111 standard concentrations were prepared of potassium hydrogen phthalate and potassium nitrate (Merck). The
112 detection limit for both parameters is approximately $1 \mu\text{M}$.

113 DOC comparability between our laboratories (relative SD: 9.3%) reproduced the previously reported range of an
114 intercalibration study (Sharp et al., 2002). Half of the deviation can be accordingly explained by day-to-day
115 variability within labs (relative SD: 2-6%, Shape et al., 2002), while the rest may be attributed to differences in
116 sample handling, storage, and fixation as described in the method section above. Overall, DOC measurements
117 from both laboratories exhibit a consistent development. Moreover, averaged initial DOC concentrations of our
118 merged dataset are within the same range as the natural DOC concentrations previously reported for the nearby
119 North Sea coastal waters during summer ($\sim 210 \mu\text{M}$, Seidel et al., 2015). This indicates that our interlab approach
120 produced plausible and reliable results.

121

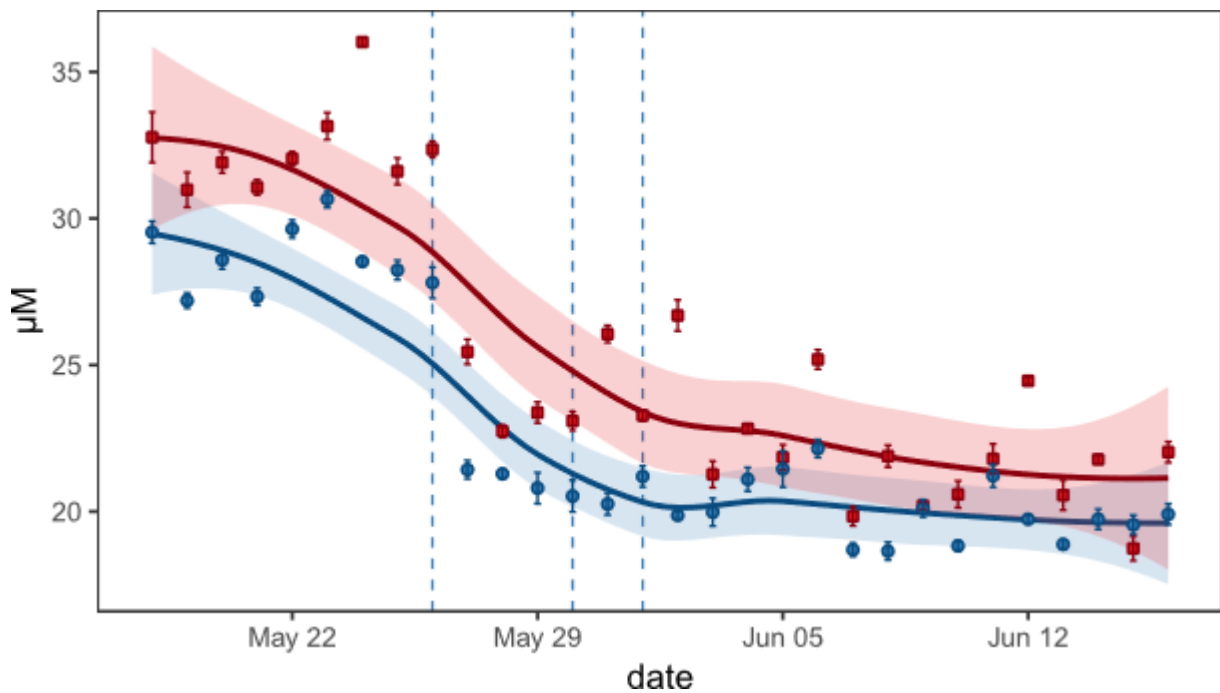


122 Figure S4 Dissolved organic carbon (DOC, $\mu\text{mol L}^{-1}$) concentrations with standard deviations between repeated
123 measurements ($n = 3 - 4$). Samples were measured at ICBM Oldenburg, Germany. measured at ICBM Oldenburg. All
124 samples are GFF filtered by default unless marked by a cross (PC).
125
126



127
128
129
130

Figure S5 Dissolved organic carbon (DOC, $\mu\text{mol L}^{-1}$) concentrations with standard deviations between repeated measurements ($n = 4$). Samples were measured at GEOMAR Kiel, Germany.

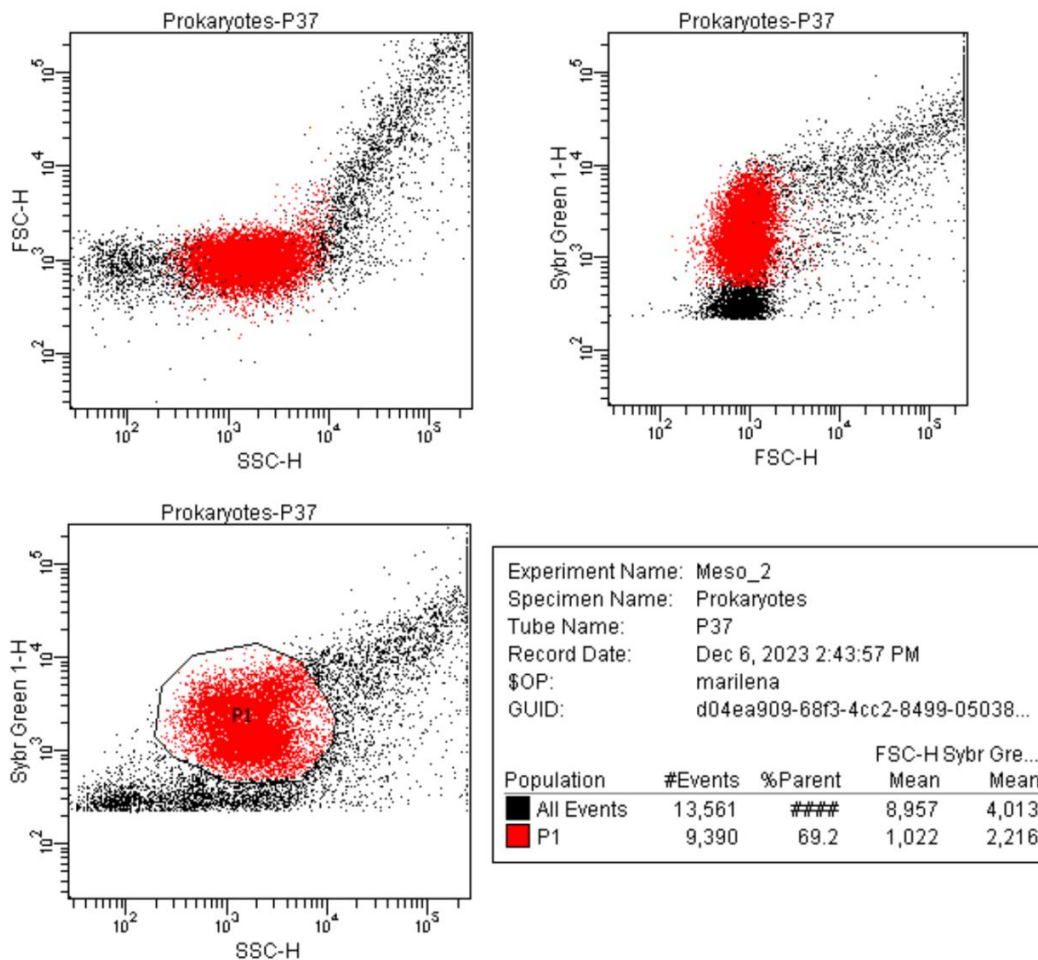


131
132
133
134
135
136
137
138
139
140
141
142
143
144
145
146
147
148
149

Figure S6 Total dissolved nitrogen (TDN, $\mu\text{mol L}^{-1}$) TDN concentrations measured at GEOMAR Kiel, Germany. TDN concentrations are shown with standard deviations between repeated measurements ($n = 4$).

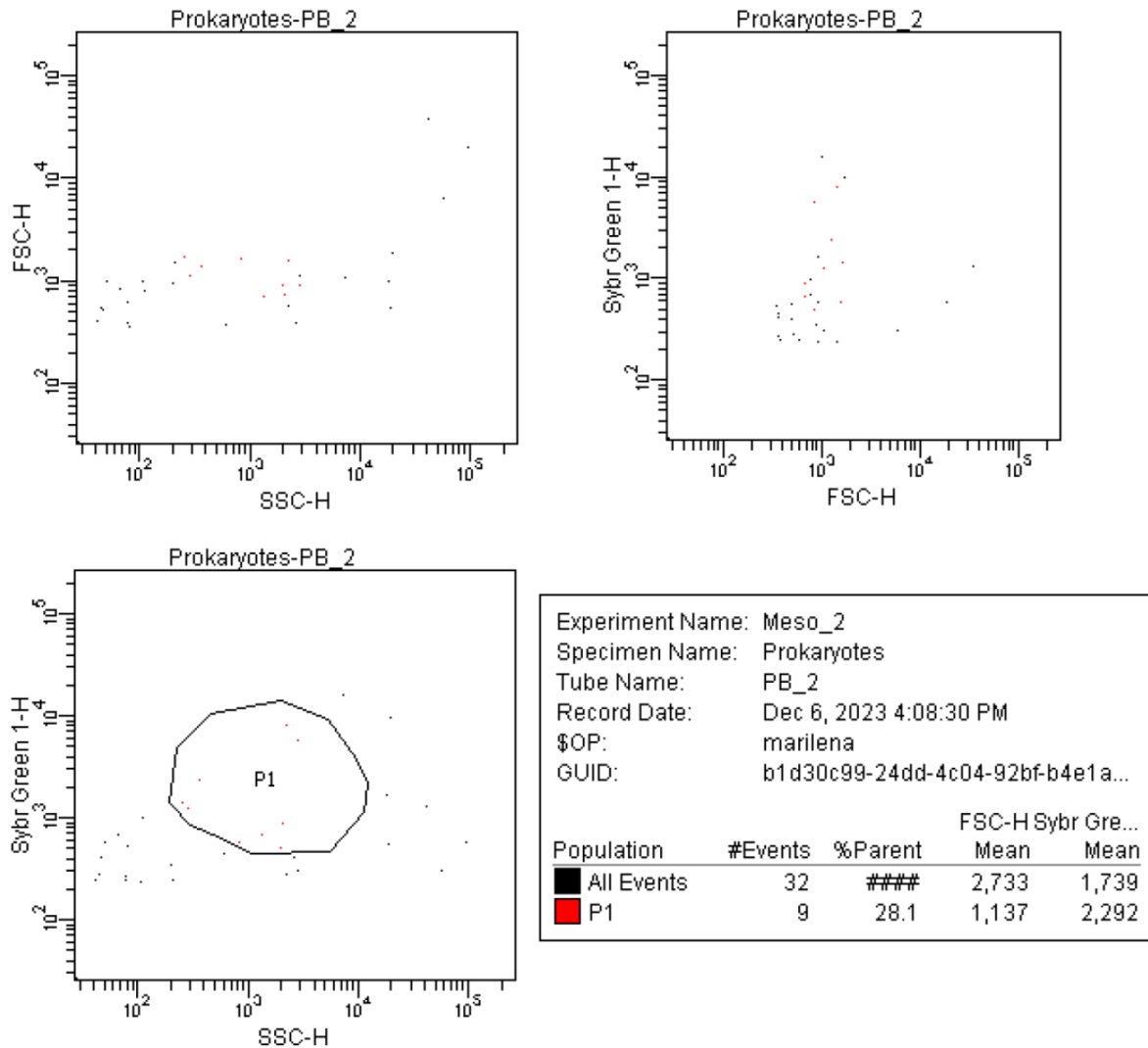
150 Sect. S4: Supporting Figures
 151
 152
 153

FACSDiva Version 6.1.3



154
 155 **Figure S7** Representative example showing flow-cytometric gating of SYBR Green I-stained prokaryotic cells (gate P1,
 156 red) from background events. The panels display (top left) forward scatter (FSC-H) versus side scatter (SSC-H), (top
 157 right) SYBR Green I fluorescence (Sybr Green 1-H) versus FSC-H, and (bottom left) SYBR Green I fluorescence versus
 158 SSC-H. Gate P1 defines the population of nucleic-acid-containing bacterial cells based on characteristic fluorescence
 159 and scatter properties, excluding non-fluorescent debris and aggregates. The same gate boundaries were applied to all
 160 experimental samples.

FACSDiva Version 6.1.3



161
 162 **Figure S8** Flow-cytometric blank control for prokaryotic gating. Example of a Milli-Q water blank stained with SYBR
 163 Green I and processed under identical conditions as environmental samples. Very few events are detected within the
 164 prokaryotic gate (P1, red), confirming the absence of significant background fluorescence or particulate contamination.
 165 Panels show (top left) FSC-H versus SSC-H, (top right) SYBR Green I fluorescence versus FSC-H, and (bottom left)
 166 SYBR Green I fluorescence versus SSC-H. The blank served to define the fluorescence threshold and verify the
 167 specificity of the gating strategy for bacterial populations.

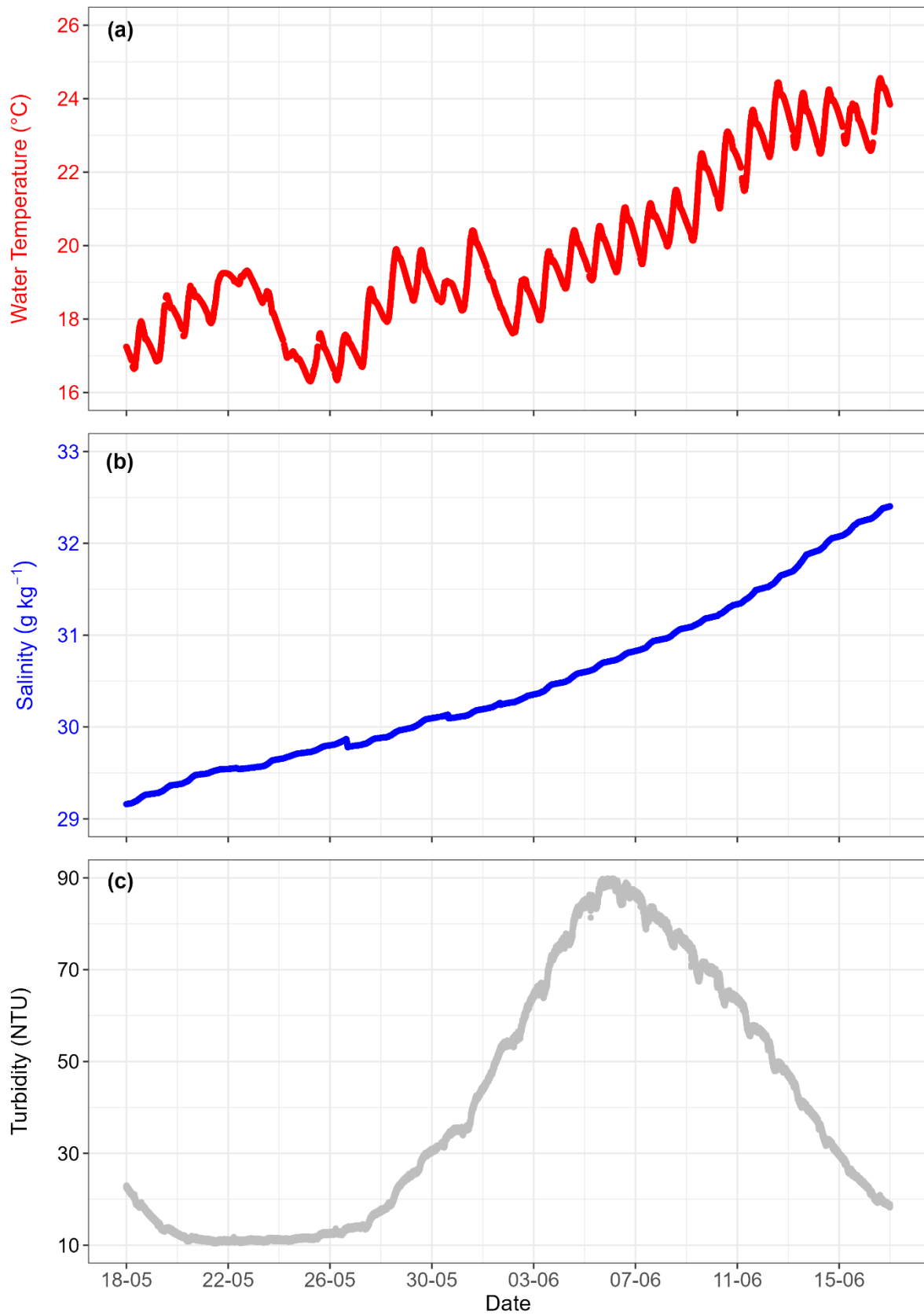
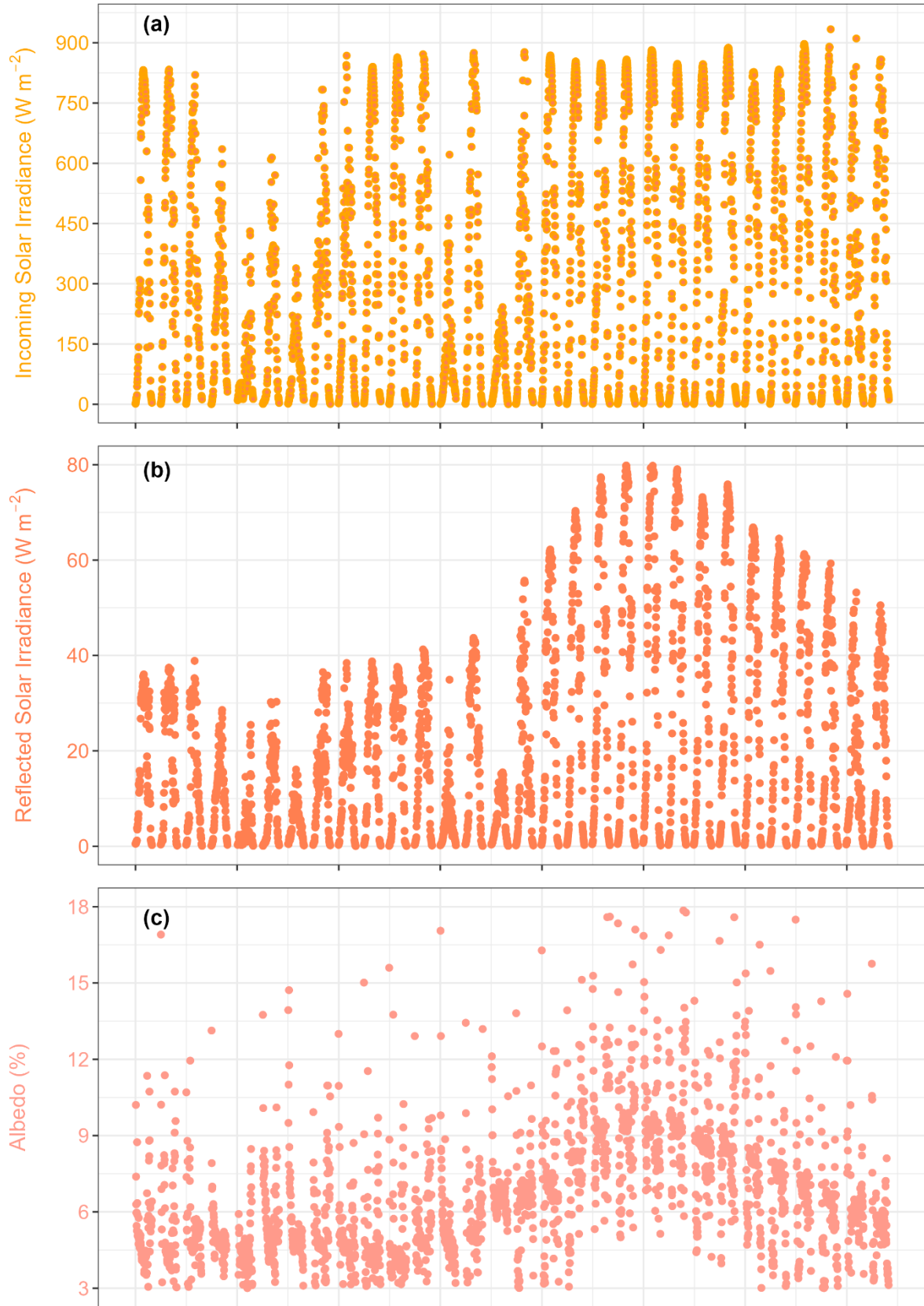
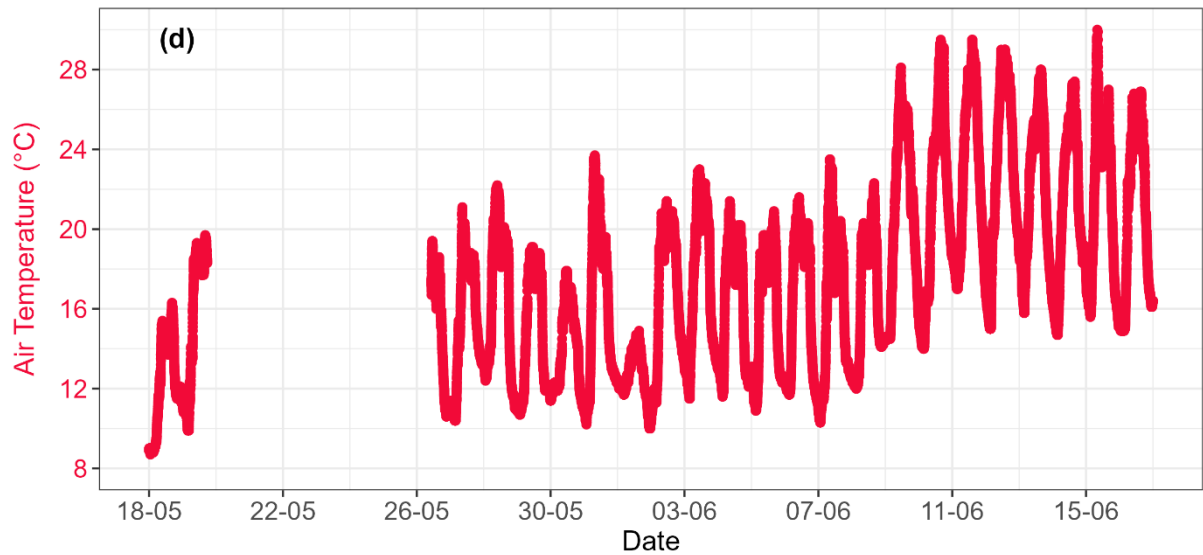


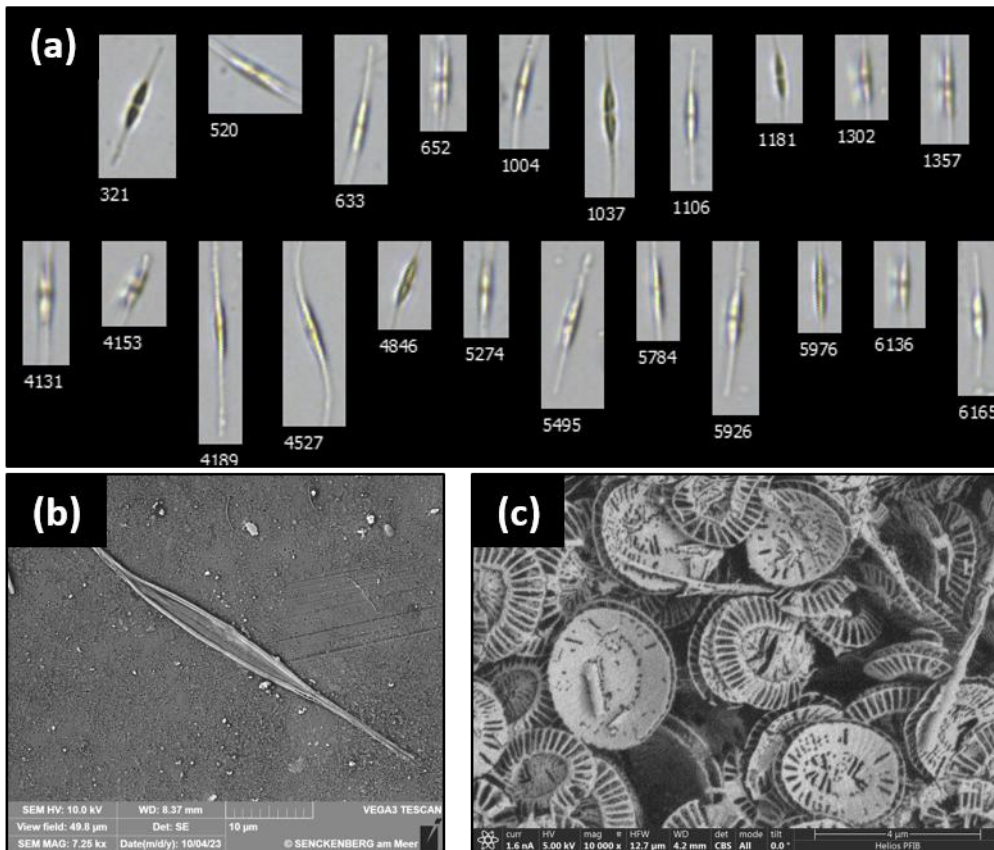
Figure S9 Time series of continuous measurements for (a) water temperature (°C), (b) salinity (g kg⁻¹), and (c) turbidity (NTU).





173

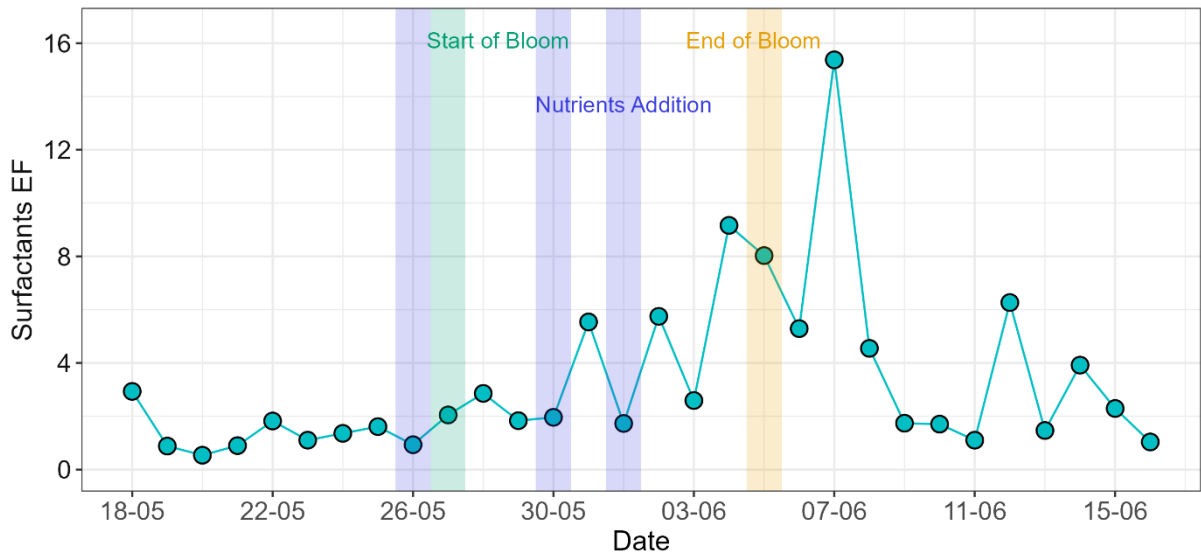
174 Figure S10 Time series of continuous measurements for (a) Incoming Solar Irradiance (W m^{-2}), (b) Reflected Solar
 175 Irradiance (W m^{-2}), (c) Albedo (%), and (d) Air Temperature ($^{\circ}\text{C}$), where gaps indicate days with missing air
 176 temperature records from the weather station.



177

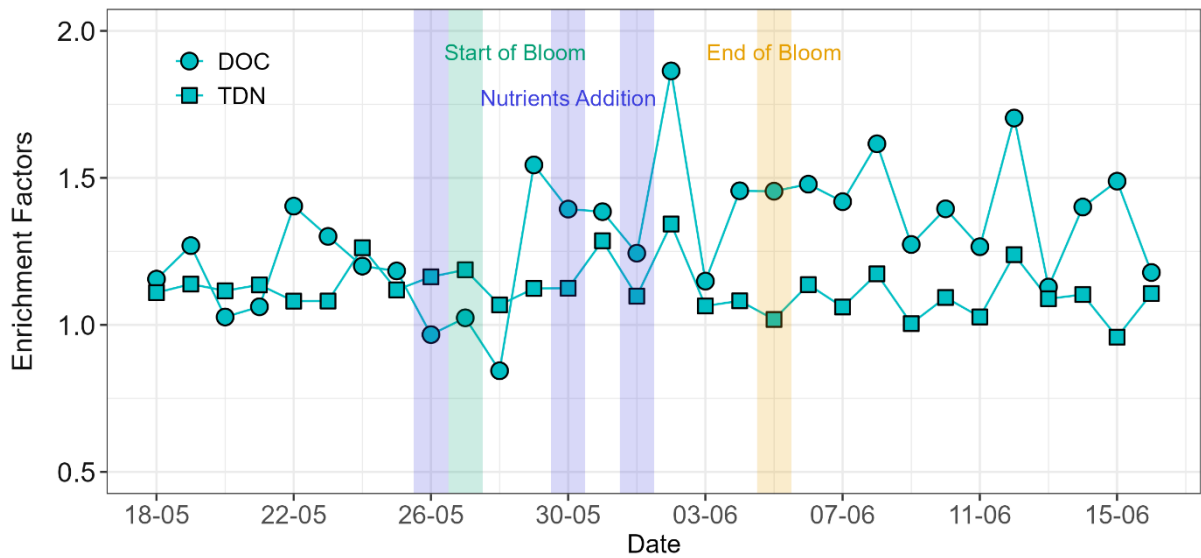
178

179 Figure S11 Bloom-forming species observed during the mesocosm experiment. (a) FlowCam images of *Cylindrotheca*
 180 *closterium* (numbers indicate image identifiers). (b) SEM image of *C. closterium*. (c) SEM image of coccoliths belonging
 181 to *Emiliana huxleyi*.



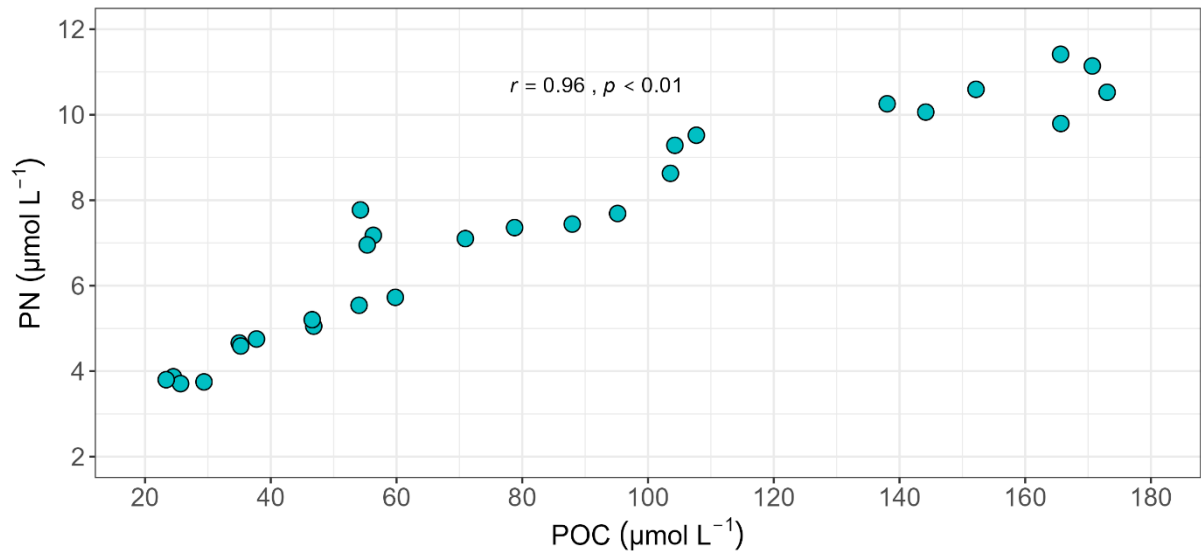
182

183 **Figure S12** Temporal variation of surfactant enrichment factor (EF) during the mesocosm. The blue highlighted parts
 184 indicate the dates of nutrients addition (May 26, May 30, and June 1), the green highlighted part indicates the start date
 185 of the bloom phase (May 27), and the yellow highlighted part indicates the end date of the bloom phase (June 5).



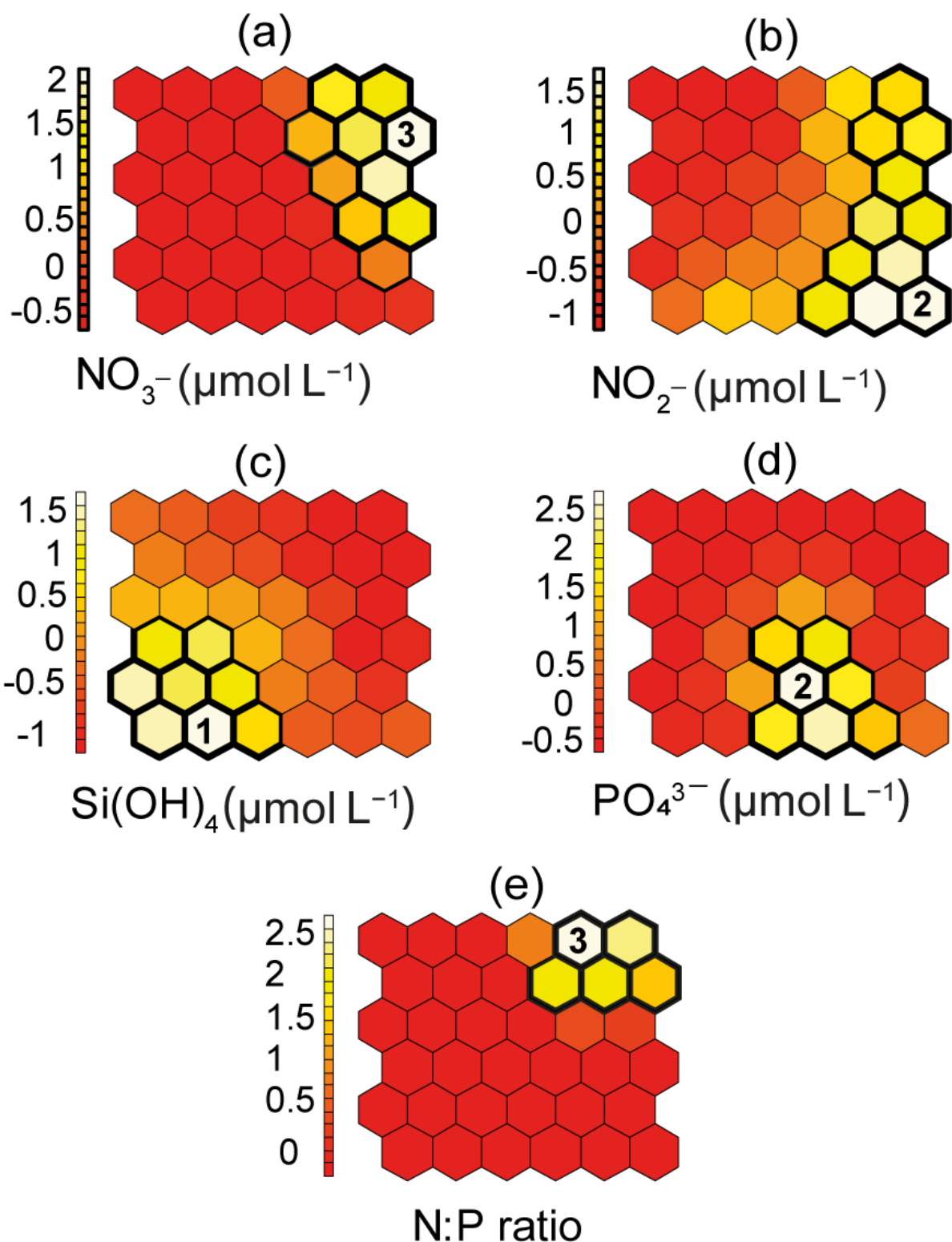
186

187 **Figure S13** Time-series of DOC (circles) and TDN (squares) enrichment factors. The blue highlighted parts indicate
 188 the dates of nutrients addition (May 26, May 30, and June 1), the green highlighted part indicates the start date of the
 189 bloom phase (May 27), and the yellow highlighted part indicates the end date of the bloom phase (June 5).



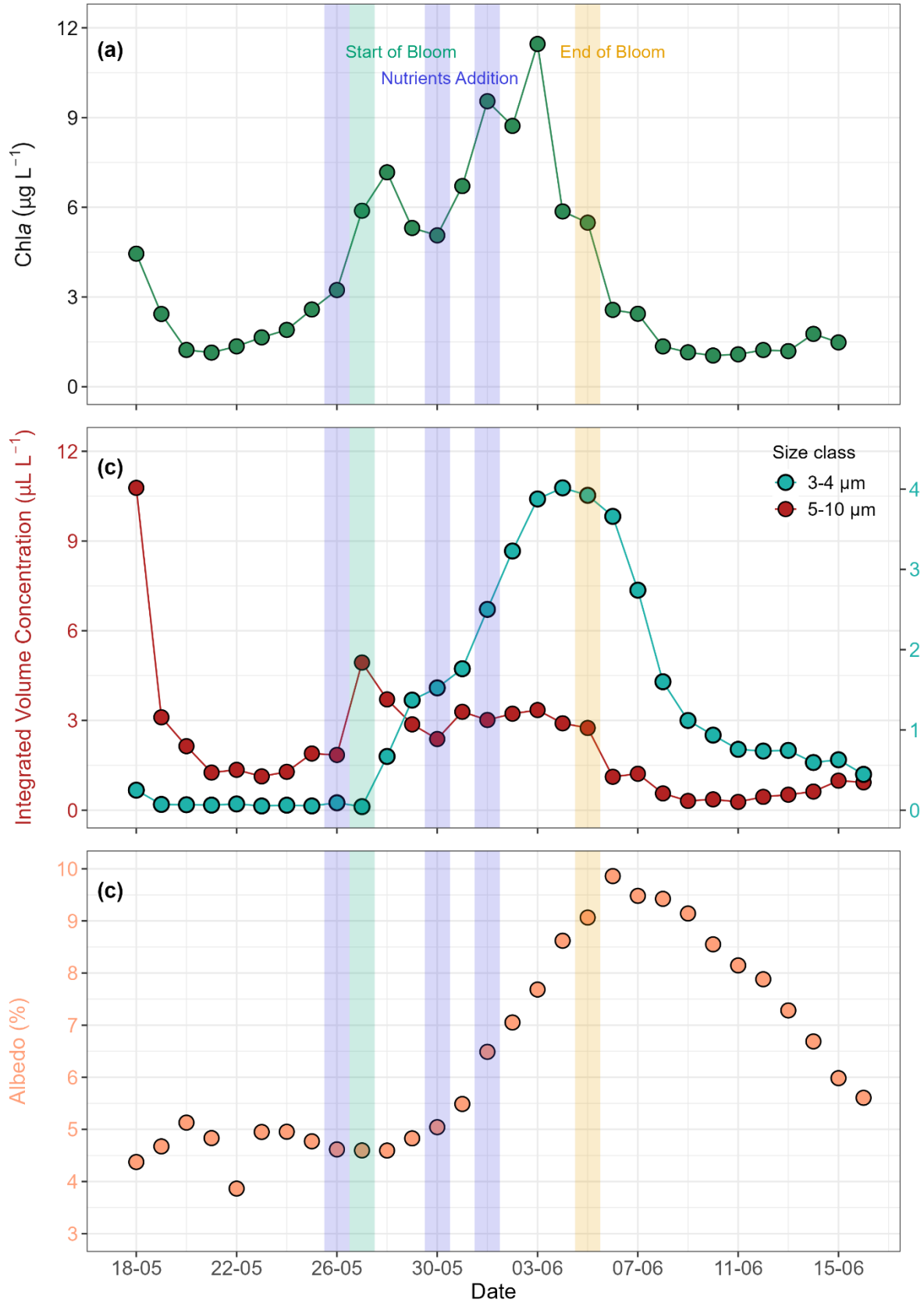
190

191 **Figure S14 Correlation between POC and PN. A strong positive relationship between POC and PN ($r = 0.96, p < 0.01$)**
192 **indicates a tight coupling of carbon and nitrogen dynamics over the time of the mesocosm.**



193

194 Figure S15 Visualization of distribution patterns and contribution of individual nutrients to the components of SOM
 195 map, (a) NO_3^- ($\mu\text{mol L}^{-1}$), (b) NO_2^- ($\mu\text{mol L}^{-1}$), (c) Si(OH)_4 ($\mu\text{mol L}^{-1}$), (d) PO_4^{3-} ($\mu\text{mol L}^{-1}$), and (e) N:P ratio. The cells
 196 labeled 1, 2, and 3 on each component plane correspond to the identified clusters in the SOM, and the bold black cells
 197 indicate the contribution of nutrients to that cluster. The degree of contribution of each nutrient is visualized by the
 198 intensity of the color of the vertical bar (light color = high contribution, dark color = low contribution). Note that the
 199 vertical bars with numbers along each component present the degree of contribution and do not measure the values of
 200 nutrients.



201

202

203

204

205

206

207

Figure S16 Temporal dynamics demonstrate key biological and physical parameters coupling during the mesocosm period. (a) Chl *a* concentration indicating phytoplankton bloom progression, (b) distribution of the particles (5–10 μm and 3–4 μm , Cells mL^{-1}) for coccolithophores, and (c) albedo (%) exhibiting increased surface reflectance during the coccolithophores bloom. The blue highlighted parts indicate the dates of nutrients addition (May 26, May 30 and June 1), the green highlighted part indicates the start date of the bloom phase (May 27), and the yellow highlighted part indicates the end date of the bloom phase (June 5).

208 **References**

- 209 Buck, M., and Himmelhaus, M.: Vibrational spectroscopy of interfaces by infrared-visible sum frequency
210 generation. *J. Vac. Sci. Tech. A*, 19, 2717-2736, 2001.
- 211 Engel, A., Sperling, M., Sun, C., Grosse, J., and Friedrichs, G.: Organic matter in the surface microlayer: Insights
212 from a wind wave channel experiment, *Frontiers in Marine Science*, 5, 182, 2018.
- 213 Korenowski, G. M., Frysinger, G. S., and Asher, W. E.: Noninvasive probing of the ocean surface using laser-based
214 nonlinear optical methods. *Photogramm. Eng. Rem. Sens.*, 59, 363-369, 1993.
- 215 Lange, F.: Investigation of Sea Surface Nanolayer Properties and Photochemistry Using Modern Laser
216 Spectroscopic and Surface Analytical Techniques, Dissertation, [https://nbn-resolving.org/urn:nbn:de:gbv:8:3-
217 2021-00564-5](https://nbn-resolving.org/urn:nbn:de:gbv:8:3-2021-00564-5), Kiel University, 2021.
- 218 Laß, K., Kleber, J., and Friedrichs, G.: Vibrational sum-frequency generation as a probe for composition, chemical
219 reactivity, and film formation dynamics of the sea surface nanolayer. *Limnol. Oceanogr.: Methods* 8, 216-228,
220 2010.
- 221 Laß, K., Friedrichs, G.: Revealing Structural Properties of the Marine Nanolayer from Vibrational Sum Frequency
222 Generation Spectra. *J. Geophys. Res.* 116, C08042, 2011.
- 223 Laß, K., Bange, H., and Friedrichs, G.: Seasonal signatures in SFG vibrational spectra of the sea surface nanolayer
224 at Boknis Eck Time Series Station (SW Baltic Sea). *Biogeosciences*, 10, 5325-5334, 2013.
- 225 Seidel, Michael, et al. Benthic-pelagic coupling of nutrients and dissolved organic matter composition in an
226 intertidal sandy beach. *Marine Chemistry*. 176,150-163, 2015.
- 227
- 228
- 229
- 230 **Sect. S5: Table S2 Average ASCD values: Biolog EcoPlate™ Substrate Utilization**

Table S2 Average substrate color development (ASCD) values for 31 carbon substrates from Biolog EcoPlate™ incub

Date	Depth	beta-Methyl-D-Glucoside	D-Galactonic Acid gamma lactone	L-Arginine	Pyruvic Acid Methyl Ester	D-Xylose	D-Galacturonic Acid	L-Asparagine
5/23/2023	SML	0.25	0.11	1.46	1.13	0.04	1.51	1.28
5/23/2023	ULW	1.24	0.88	1.39	0.98	0.36	1.03	1.26
5/26/2023	SML	0.47	0.64	1.06	1.59	0.10	1.31	1.65
5/26/2023	ULW	-0.03	0.25	0.91	2.15	0.30	0.07	1.36
5/27/2023	SML	0.82	0.23	1.12	1.07	0.42	1.20	1.40
5/27/2023	ULW	-4.61	26.18	-12.65	-11.38	30.59	11.37	-26.70
5/30/2023	SML	0.24	0.41	1.16	1.24	0.24	1.35	1.73
5/30/2023	ULW	1.26	0.83	1.16	1.08	0.91	1.10	0.86
5/31/2023	SML	1.15	0.92	0.81	1.12	0.59	1.09	1.40
5/31/2023	ULW	2.85	7.75	3.43	-0.98	3.89	-2.99	-1.78
6/3/2023	SML	0.73	1.06	1.07	1.12	1.09	1.09	1.19
6/3/2023	ULW	0.76	0.97	1.43	2.90	0.42	0.86	1.19
6/4/2023	SML	0.74	0.78	1.19	1.11	0.81	1.03	1.32
6/4/2023	ULW	1.19	0.97	1.05	2.23	1.00	1.09	1.48
6/7/2023	SML	0.81	1.05	1.07	0.62	1.57	1.34	0.67
6/7/2023	ULW	0.85	1.94	2.06	5.78	0.17	0.44	1.45
6/8/2023	SML	0.74	1.06	1.10	0.90	0.78	1.38	1.71
6/8/2023	ULW	0.59	0.95	1.04	0.96	0.21	1.13	0.91
6/11/2023	SML	0.53	1.58	1.42	0.43	1.03	0.51	1.70
6/11/2023	ULW	0.68	0.98	1.07	2.28	0.34	0.63	1.00
6/12/2023	SML	0.61	1.34	1.23	0.96	0.79	0.43	1.85
6/12/2023	ULW	0.00	1.57	1.42	1.99	-0.21	0.37	2.64

ations, used to assess microbial carbon utilization in SML and ULW samples. Negative values reflect negligible or no :

Tween 40	I-Erythritol	2-Hydroxy Benzoic Acid	L-Phenylalanine	Tween 80	D-Mannitol	4-Hydroxy Benzoic Acid	L-Serine	alpha-Cyclodextrin
1.18	1.14	0.14	0.35	1.21	1.70	0.51	1.70	2.45
1.37	0.79	0.46	0.87	0.52	3.15	0.25	1.18	2.34
1.17	0.26	-0.02	0.59	1.30	1.77	-0.03	2.05	2.02
1.32	-0.06	-0.18	0.47	1.26	3.02	-0.67	2.11	3.69
1.33	0.88	-0.01	0.91	1.32	1.57	-0.05	1.85	1.57
0.90	10.58	14.74	11.04	8.52	-13.59	16.62	-17.45	-25.07
1.23	0.13	-0.01	0.98	0.88	2.10	-0.03	2.18	2.34
1.47	0.94	0.71	2.10	0.06	-0.28	2.30	0.61	2.32
1.20	1.15	-0.14	0.80	1.38	1.97	-0.18	1.41	1.94
12.45	5.48	8.25	-6.72	7.70	1.70	-11.40	3.02	2.68
1.19	1.04	-0.19	1.05	1.11	1.87	0.03	1.64	1.84
0.90	1.24	0.40	0.28	0.47	2.26	-0.49	1.55	3.34
0.98	1.24	0.03	0.38	1.29	1.73	0.63	1.35	1.57
0.88	0.45	0.26	1.19	0.80	1.49	-0.10	1.36	1.21
1.22	1.06	-0.11	0.15	1.16	2.10	0.86	1.27	2.00
1.55	0.47	1.20	0.36	-0.97	0.78	-1.41	0.50	3.12
1.17	0.56	-0.02	1.10	1.37	1.90	-0.11	1.73	1.69
1.23	0.14	-0.13	0.91	0.50	1.86	0.26	1.63	2.64
1.64	0.31	-0.06	1.12	1.62	2.32	0.13	1.22	1.53
0.93	0.59	-0.06	0.93	0.81	2.73	0.55	1.10	2.28
1.23	0.09	-0.15	0.55	1.22	2.25	-0.16	1.87	2.27
0.84	0.96	-0.88	-1.97	0.05	1.40	-2.78	2.87	5.59

substrate use and were retained for transparency.

N-Acetyl-D-Glucosamine	gamma-Hydroxybutyric Acid	L-Threonine	Glycogen	D-Glucosaminic Acid	Itaconic Acid	Glycyl-L-Glutamic Acid	D-Cellobiose	Glucose-1-Phosphate
1.79	0.86	1.76	1.91	0.35	1.15	1.47	1.50	0.58
0.66	0.08	1.70	3.32	0.78	0.10	1.58	1.69	0.51
1.97	0.92	1.26	1.80	0.15	0.75	1.42	2.26	1.18
3.74	0.48	1.35	3.22	0.08	0.85	0.52	1.70	0.31
1.81	1.15	1.83	1.62	0.11	0.15	1.55	1.88	1.20
-16.81	38.98	-16.09	-49.17	-2.50	9.40	-14.46	-12.10	30.93
2.08	1.40	1.78	1.94	0.23	0.23	1.42	1.87	1.35
0.36	2.72	1.85	0.87	-0.34	1.07	0.06	2.23	1.11
1.65	1.48	1.94	1.43	0.23	0.46	1.34	1.61	1.04
-4.27	-5.07	3.93	4.01	5.56	-1.26	3.74	4.90	-2.68
1.50	1.63	1.69	1.51	0.20	0.60	1.18	1.67	1.38
1.03	0.95	1.05	3.04	0.17	-0.59	0.95	0.97	0.95
1.34	1.46	1.74	1.05	1.11	1.03	1.16	1.39	1.01
1.33	0.25	1.49	2.65	0.73	0.59	1.00	1.97	1.45
1.64	1.35	1.84	1.03	0.35	1.06	1.11	1.08	0.91
3.84	-3.07	1.57	5.02	0.76	0.13	0.39	1.19	0.90
1.76	1.21	1.94	1.16	0.09	0.29	1.35	1.50	0.97
2.01	0.69	1.43	2.48	0.56	1.04	0.92	1.58	1.24
1.81	1.79	1.85	1.29	0.08	0.28	1.36	1.54	0.53
2.05	0.23	1.13	2.37	0.78	0.64	0.96	0.67	0.94
1.88	1.19	2.27	1.53	-0.05	0.48	1.48	1.70	1.18
3.17	-2.47	1.89	5.90	-1.13	-0.33	0.57	1.84	2.19

alpha-Ketobutyric Acid	Phenylethylamine	alpha-D-Lactose	D,L-alpha-Glycerol Phosphate	D-Malic Acid	Putrescine
0.76	-0.04	0.87	0.61	0.50	0.80
-0.04	-0.35	0.49	0.50	1.19	0.71
0.23	0.01	0.29	0.60	0.88	1.34
0.14	-0.12	0.96	0.95	0.01	0.85
0.39	0.07	0.59	0.65	0.98	1.39
29.02	9.78	18.89	2.44	-12.71	-3.69
0.24	0.05	0.04	0.63	0.22	1.34
1.25	0.82	-0.48	0.22	0.01	1.83
0.26	0.01	0.95	0.51	0.21	1.29
-4.50	-4.33	-6.35	-0.28	4.29	-2.02
0.21	0.26	-0.02	0.51	0.43	1.32
0.31	0.18	0.58	1.26	0.71	0.98
0.32	0.35	0.49	0.37	0.76	1.26
0.49	-0.06	0.08	0.85	0.41	1.23
0.10	-0.05	1.04	0.55	1.03	1.12
-1.50	0.30	0.76	1.00	0.61	0.82
0.30	0.22	0.51	0.47	0.98	1.19
0.53	0.13	0.82	1.32	0.56	0.87
0.22	0.22	0.78	0.23	0.70	1.29
0.49	0.32	0.52	0.94	0.95	1.18
0.13	-0.19	0.34	0.35	1.02	1.30
0.82	-0.73	0.57	0.44	0.62	3.77